Antarctic Science 15 (4): 547–555 (2003) © Antarctic Science Ltd Printed in the UK DOI: 10.1017/S095410200301664

Surface "waves" on Byrd Glacier, Antarctica

D. REUSCH[1] and T. HUGHES[2]

[1]*Department of Natural Sciences, 173 High Street, University of Maine at Farmington, Farmington, ME 04938, USA*
[2]*Department of Earth Sciences, Climate Change Institute, University of Maine, Orono, ME 04473, USA*

Abstract: Byrd Glacier has one of the largest ice catchment areas in Antarctica, delivers more ice to the Ross Ice Shelf than any other ice stream, and is the fastest of these ice streams. A force balance, combined with a mass balance, demonstrates that stream flow in Byrd Glacier is transitional from sheet flow in East Antarctica to shelf flow in the Ross Ice Shelf. The longitudinal pulling stress, calculated along an ice flowband from the force balance, is linked to variations of ice thickness, to the ratio of the basal water pressure to the ice overburden pressure where Byrd Glacier is grounded, and is reduced by an ice-shelf buttressing stress where Byrd Glacier is floating. Longitudinal tension peaks at pressure-ratio maxima in grounded ice and close to minima in the ratio of the pulling stress to the buttressing stress in floating ice. The longitudinal spacing of these tension peaks is rather uniform and, for grounded ice, the peaks occur at maxima in surface slope that have no clear relation to the bed slope. This implies that the maxima in surface slope constitute a "wave train" that is related to regular variations in ice-bed coupling, not primarily to bed topography. It is unclear whether these surface "waves" are "standing waves" or are migrating either upslope or downslope, possibly causing the grounding line to either retreat or advance. Deciding which is the case will require obtaining bed topography in the map plane, a new map of surface topography, and more sophisticated modeling that includes ice flow linked to subglacial hydrology in the map plane.

Received 17 January 2003, accepted 5 August 2003

Key words: East Antarctica, ice stream, outlet glacier, Ross embayment, unstable ice flow

Introduction

Byrd Glacier (80.3°S, 160°W) drains one of the largest ice catchment areas in Antarctica (Hughes 1998, fig. 3.7; Rignot & Jacobs 2002). As seen in Fig. 1, East Antarctic ice becomes a strongly convergent sheet flow as it approaches Byrd Glacier, becomes a linear stream flow as it enters a fjord through the Trans-Antarctic Mountains, and ends as a diverging shelf flow as it enters the Ross Ice Shelf (Jezek 1998). Several tributaries of stream flow can be seen developing in the region of converging sheet flow in Fig. 2. Wind scour and sublimation in the fjord remove winter snow and expose bare ice, seen as a white surface in Fig. 2. Byrd Glacier becomes afloat about halfway through the fjord and merges with the Ross Ice Shelf over a distance of 50 to 100 km beyond the fjord, as seen by the abatement of shear and tensile crevasses along its sides over this distance in Fig. 2. A nearly continuous bottom reflection was obtained from radio-echo sounding along the ice flowband shown in Fig. 3, when an LC-130 aircraft flew only 300 ft above the ice. The ice top and bottom reflections are shown in Fig. 4. This led to two attempts to model the dynamics of Byrd Glacier, based on the radio-echo data and on field measurements of surface mass balance, velocities, and elevations in 1978–79 (Hughes 1979, Hughes & Fastook 1981, Brecher 1982). These modelling studies, by Whillans *et al*. (1989) and by Scofield *et al*. (1991), did not investigate the reason for the sequence of changes in ice surface slope that gives the appearance of surface "waves" for grounded ice (ice upslope from the grounding zone, GZ in Fig. 3). As seen in Fig. 3, these "waves" have no clear relationship to bed topography. The "waves" extend

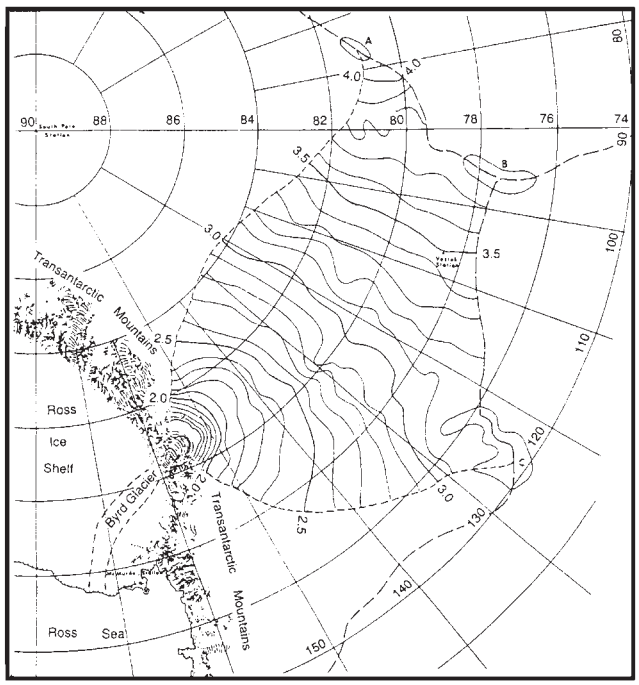

Fig. 1. Byrd Glacier and its ice drainage system. Ice elevations contoured at 0.1 km intervals.

https://doi.org/10.1017/S0954102003001664 Published online by Cambridge University Press

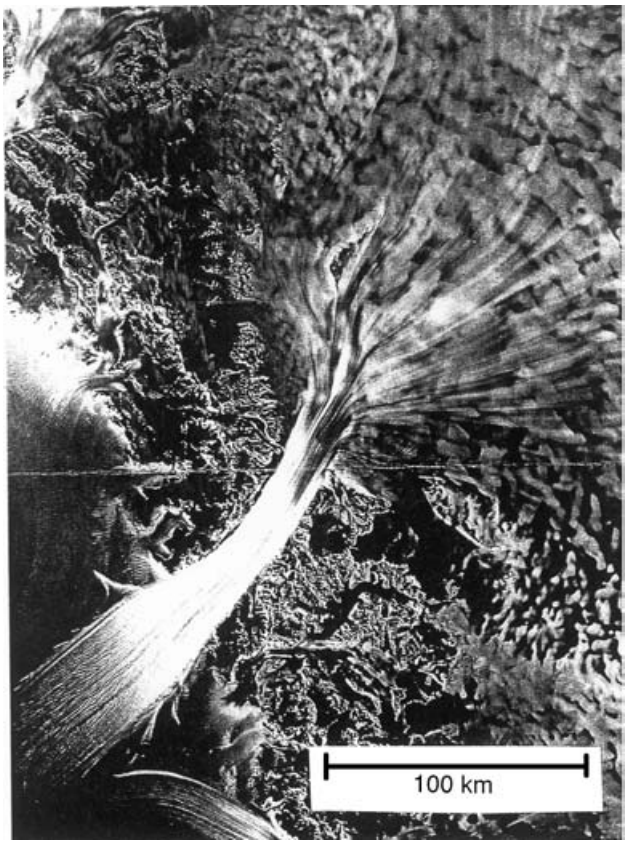

Fig. 2. A Radarsat image of Byrd Glacier (Jezek 1998). The Transantarctic Mountains (upper left to lower right) separate the East Antarctic Ice Sheet (top) from the Ross Ice Shelf (bottom). North is at the bottom, as in the standard Antarctic orientation.

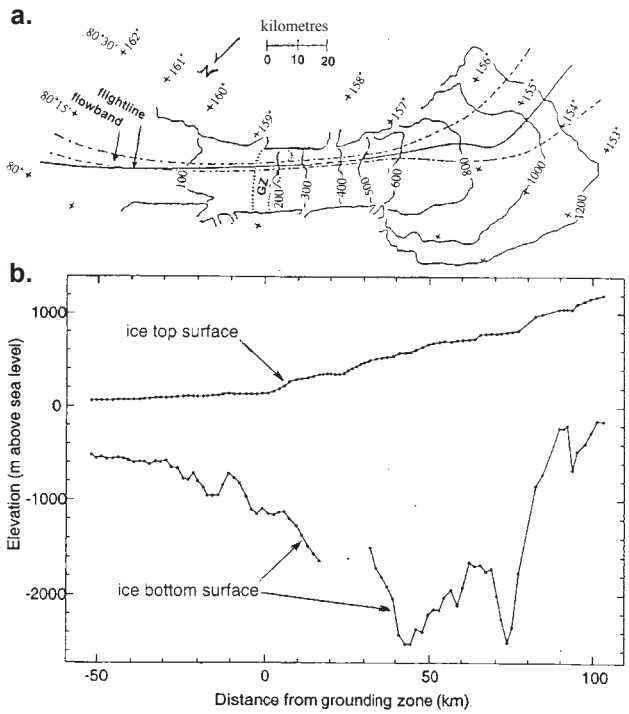

Fig. 3. The only radio-echo flightline giving a nearly continuous bottom reflection for Byrd Glacier. **a.** The flightline (solid line) is shown in relation to the ice flowband (dashed lines) used in this study. GZ is the grounding zone according to Scofield (1988). **b.** Top and bottom reflections along the radio-echo flightline.

transversely between the lateral shear zones of Byrd Glacier (Brecher 1982). Investigating the physical basis for these waves is the purpose of this study.

Modelling approach

Our study combines the mass balance developed by Van der Veen (1983, 1999, pp. 162–167) with the force balance presented by Hughes (1992, 1998, pp. 51–61 and 168–173). A vertical ice column of length Δx and width w has a horizontal base that touches the sloping bed where the column height h_I gives ice overburden pressure P_I and where basal pressure P_W would support a water column of height h_W. At upslope distance Δx, these heights are $h_I + \Delta h$ and $h_W + \Delta h_W$, where Δh_W can be positive or negative. For respective ice and water densities ρ_I and ρ_W, ice of height $(\rho_W/\rho_I)h_W$ would float in water of depth h_W. Higher ice is grounded on, and supported by, the bed. Our coordinates have their origin at sea level in the middle of the flowband and the middle of grounding zone GZ in Fig. 3. In our model, x is horizontal and positive in the upslope direction along the centreline of the flowband, y is horizontal and follows ice elevation contour lines, and z is vertical and positive upward. With x = 0 at the grounding line, taken as the middle of the grounding zone, horizontal distances (kilometres) along x, positive upslope and negative downslope (both positive in our model), are as shown in Fig. 3.

We want to match the measured surface slope in Fig. 3 with surface slope $\Delta h/\Delta x$ calculated as the change Δh in surface elevation h in successive incremental lengths Δx along longitudinal horizontal distance x upslope from the grounding line. Along the flowband, w is flowband width, h_I is ice thickness, $h_R = h - h_I$ is bedrock height above (positive) or depth below (negative) sea level, u is the measured ice velocity and is assumed to be constant through h_I, u_x and u_y are the respective velocities of flowband longitudinal extension or compression and transverse narrowing or widening, $w = w_0$, $h_I = h_0$, and $u = u_0$ at the grounding line where x = 0, a is the average surface and basal ice accumulation or ablation rate, ρ_I is ice density, ρ_W is water density, g is acceleration due to gravity, θ is the angle of divergence or convergence of ice flow in distance Δx such that $\tan\theta = \Delta w/\Delta x$.

Let τ_O and τ_S be shear stresses along the sides and at the base of the flowband, respectively. As shown by Hughes (1998, p. 51–55), the force balance gives for the longitudinal deviatoric tensile stress σ_T arising from the freeboard ice height $h_I(1 - \rho_I/\rho_W)$ that is not buttressed

https://doi.org/10.1017/S0954102003001664 Published online by Cambridge University Press

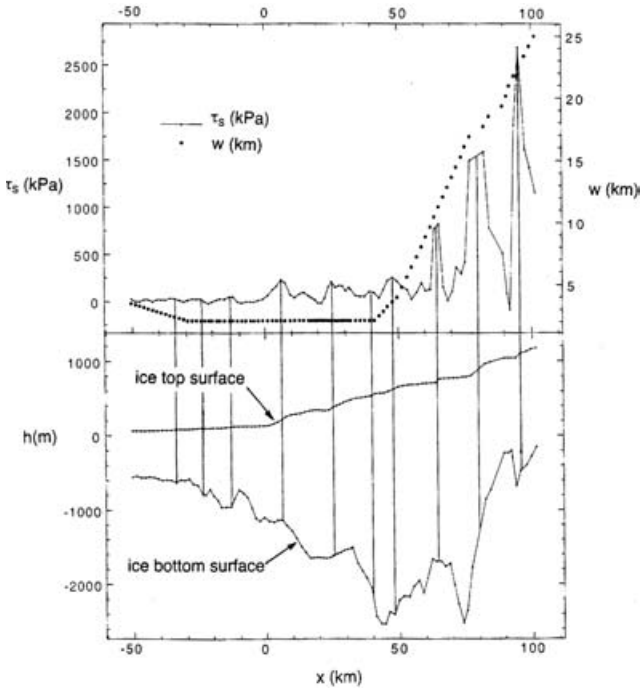

Fig. 4. Variations of side shear stress needed to produce the observed surface slopes along Byrd Glacier if side shear is the dominant stress. Top: Variations of side shear stress τ_S and width w of the flowband in Fig. 3. Bottom: Surface and basal ice profiles along the flightline in Fig. 3.

$$\sigma_T = \frac{\rho_I g h_I}{2 + \left(\dot{\varepsilon}_{yy} / \dot{\varepsilon}_{xx}\right)} \left(1 - \frac{\rho_I}{\rho_W}\right) \left(\frac{P_W}{P_I}\right)^2 \tag{1}$$

where $\dot{\varepsilon}_{xx}$ and $\dot{\varepsilon}_{yy}$ are the respective longitudinal and transverse strain rates measured by Scofield (1988) and by Whillans *et al*. (1989), P_W is the basal water pressure, and P_I is the ice overburden pressure at the bed. Then surface slope $\Delta h/\Delta x$ is obtained by combining the force balance and the mass balance for steady-state flow of ice downslope in the negative x direction (Hughes 1998, p. 55):

$$\frac{\Delta h}{\Delta x} = \left(1 - \frac{\rho_I}{\rho_W}\right)\left(\frac{P_W}{P_I}\right)^2 \left\{ \frac{w h_i a}{awx + w_0 h_0 u_0} - \frac{w h_I^2 R \cos\theta}{awx + w_0 h_0 u_0} \left[\frac{\rho_I g h_I}{2A} \left(1 - \frac{\rho_I}{\rho_W}\right)\left(\frac{P_W}{P_I}\right)^2 \right]^n \right.$$

$$\left. - \frac{w h_I^2}{awx + w_0 h_0 u_0} \left[\left(\frac{\partial u_y}{\partial y}\right) \sin\theta + \left(\frac{\partial u_x}{\partial y}\right) \cos\theta + \left(\frac{\partial u_y}{\partial x}\right) \sin\theta \right] \right\} \tag{2}$$

$$+ \frac{h_I}{w} \left[1 + \frac{1}{2} \left(1 - \frac{\rho_I}{\rho_W}\right)\left(\frac{P_W}{P_I}\right)^2 \right] \tan\theta + h_I \left(1 - \frac{\rho_I}{\rho_W}\right)\left(\frac{P_W}{P_I}\right) \frac{\Delta}{\Delta x}\left(\frac{P_W}{P_I}\right) + \frac{2 h_I \tau_S + w \tau_O}{\rho_I g w h_I}$$

Ratio P_W/P_I is a major variable in Eqs 1 & 2, where $P_W = \rho_W g h_W$ and $P_I = \rho_I g h_I$. It appears because σ_T in Eq. 1 is included in the force balance leading to Eq. 2. In Eq. 1, $\sigma_T = \sigma_{xx} - \sigma_{zz}$ is tensile when $\dot{\varepsilon}_{xx}$ is a longitudinal extending strain rate because longitudinal stress σ_{xx} is then less compressive than vertical stress σ_{zz}. The longitudinal gradient of P_W/P_I is $\Delta(P_W/P_I)/\Delta x$, and it is also included in the force balance. In Eq. 2, R is an invariant that includes the contributions of strain rates $\dot{\varepsilon}_{xx}$, $\dot{\varepsilon}_{yy}$, $\dot{\varepsilon}_{xy}$, and $\dot{\varepsilon}_{xz}$ to creep in ice related to Cartesian coordinates x, y, z (Thomas 1973a, 1973b). For $\dot{\varepsilon}_{xx}$ (Hughes 1998, p. 54):

$$R = \frac{\left[1 + \left(\dot{\varepsilon}_{yy}/\varepsilon_{xx}\right) + \left(\dot{\varepsilon}_{yy}/\dot{\varepsilon}_{xx}\right)^2 + \left(\dot{\varepsilon}_{xy}/\dot{\varepsilon}_{xx}\right)^2 + \left(\dot{\varepsilon}_{xz}/\dot{\varepsilon}_{xx}\right)^2\right]^{\frac{n-1}{2}}}{\left[2 + \left(\dot{\varepsilon}_{yy}/\dot{\varepsilon}_{xx}\right)\right]^n}$$

$$= \frac{\left(\sigma_c / \sigma'_{xx}\right)^{n-1}}{\left[2 + \left(\dot{\varepsilon}_{yy}/\dot{\varepsilon}_{xx}\right)\right]^n} \tag{3}$$

where $\sigma'_{xx} = (\sigma_{xx} - \sigma_{zz})/2 = \sigma_T/2$ is the longitudinal deviator stress and σ_c is the effective creep stress. In Eq. 2, A and n are the respective hardness and viscoplastic parameters in the Glen (1955) flow law for ice that, using the standard tensor notation for axes i, j in Cartesian coordinates x, y, z, relates strain rate component $\dot{\varepsilon}_{ij}$ to deviator stress component σ'_{ij} and effective creep stress σ_c (Nye 1953):

$$\dot{\varepsilon}_{ij} = \left(\sigma_c^{n-1} / A^n\right) \sigma'_{ij} \tag{4}$$

Steady-state flow is assumed, because there has been no measurable change in ice surface elevation between the 1960–1961 and the 1978–1979 Antarctic summers (Brecher 1982).

Equation 2 can be solved for $\Delta(P_W/P_I)/\Delta x$ if Byrd Glacier has a rock floor so that basal sliding obeys the Weertman (1957a) sliding law modified for stream flow (Hughes 1998, p. 57 and pp. 105–106):

$$u_s = \left[\frac{\tau_O}{B\left(1 - P_W / P_I\right)^2} \right]^m \tag{5}$$

where B and m are the respective basal sliding and ice creep parameters and u_s is the magnitude of the basal sliding velocity. Solving Eq. 5 for τ_O:

$$\tau_O = B\left(1 - P_W / P_I\right)^2 u_s^{1/m} \tag{6}$$

Equation 6 reduces to the Weertman (1957a) equation when P_W/P_I is negligible for sheet flow (for which basal water is only a thin film that wets bedrock, so it does not rise in a borehole), and $\tau_O = 0$ when $P_W/P_I = 1$ for shelf flow (for which basal water drowns all bedrock bumps, except at ice rises and ice rumples). Therefore, Eq. 6 applies for stream flow in which $0 < P_W/P_I < 1$. Paterson (1994), Hooke (1998), and Van der Veen (1999) discuss various treatments of basal sliding. It turns out that the treatment of basal sliding is not critical to our analysis because $\tau_O << \sigma_T$ except when P_W/P_I is negligible

https://doi.org/10.1017/S0954102003001664 Published online by Cambridge University Press

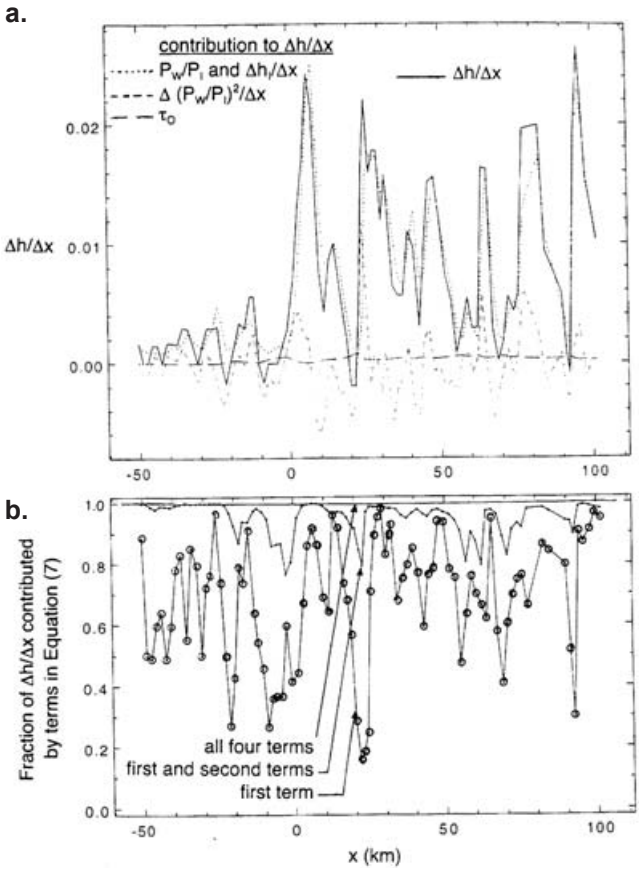

Fig. 5. Contributions of the terms in Eq. 7 to the surface slope of Byrd Glacier along the flightline in Fig. 2. The first term contains the effects of pressure ratio P_W/P_I and variations in ice thickness h_I. The second term contains the effects of pressure gradient $\Delta(P_W/P_I)^2/\Delta x$. The third term contains side shear stress τ_S and has no effect on this scale. The fourth term contains the effects of variations in P_W/P_I and sliding velocity u_s on basal shear stress τ_O. These effects are shown in two ways: **a.** The observed surface slope (thick line) is the sum of surface slopes produced by the first term (thin line of short dashes), the second term (thin line of medium dashes), and the fourth term (thin line of long dashes). Note that the second term, containing $\Delta(P_W/P_I)^2/\Delta x$, typically makes both positive and negative contributions to the surface slope. **b.** Using the vertical axis as a scale only, the fractional contributions to surface slope are given by the connected circled dots for the first term, the connected dots for the first and second terms, and the top straight line (100%) for the first, second, third, and fourth terms. This shows that the first term generally contributes about 70% and the first and second terms generally contribute about 95%.

For the flowband in Fig. 3, velocity gradients and strain rates calculated by Scofield (1988), Whillans *et al*. (1989), and Zhao (1990) from the surface velocity data show that at least within the fjord the terms containing velocity gradients $\partial u_y/\partial y$, $\partial u_x/\partial y$, and $\partial u_y/\partial x$ can be ignored, $R \approx 2^{-n}$, and $\tan\theta \approx 1$ in Eq. 2. With these simplifications, substituting Eq. 6 for τ_O, and noting that $awx << w_0h_0u_0$ because a is negligible over distance $x < 100$ km for Byrd Glacier grounded in the fjord, Eq. 2 becomes to a good approximation:

$$\frac{\Delta h}{\Delta x} = -\frac{wh_I^2}{w_0h_0u_0}\left(\frac{\rho_I g h_I}{4A}\right)^n\left(1-\frac{\rho_I}{\rho_W}\right)^{n+1}\left(\frac{P_W}{P_I}\right)^{2n+2} + h_I\left(1-\frac{\rho_I}{\rho_W}\right)\left(\frac{P_W}{P_I}\right)\frac{\Delta}{\Delta x}\left(\frac{P_W}{P_I}\right) + \frac{2\tau_S}{\rho_I g w} + \frac{u_s^{1/m}B}{\rho_I g h_I}\left(1-\frac{P_W}{P_I}\right)^2 \quad (7)$$

Solving Eq. 7 for $\Delta(P_W/P_I)/\Delta x$, the longitudinal gradient of P_W/P_I:

$$\frac{\Delta}{\Delta x}\left(\frac{P_W}{P_I}\right) = \left[\frac{wh_I}{w_0h_0u_0}\left(\frac{\rho_I g h_I}{4A}\right)^n\left(1-\frac{\rho_I}{\rho_W}\right)^n\right]\left(\frac{P_W}{P_I}\right)^{2n+1}$$

$$+\left[-h_I^{-1}\left(\frac{2\tau_S}{\rho_I g w} + \frac{u_s^{1/m}B}{\rho_I g h_I} - \frac{\Delta h}{\Delta x}\right)\left(1-\frac{\rho_I}{\rho_W}\right)^{-1}\right]\left(\frac{P_W}{P_I}\right)^{-1}$$

$$+\left[-\frac{u_s^{1/m}B}{\rho_I g h_I^2}\left(1-\frac{\rho_I}{\rho_W}\right)^{-1}\right]\left(\frac{P_W}{P_I}\right) + \left[\frac{2u_s^{1/m}B}{\rho_I g h_I^2}\left(1-\frac{\rho_I}{\rho_W}\right)^{-1}\right]$$

$$= C_1\left(\frac{P_W}{P_I}\right)^{2n+1} + C_2\left(\frac{P_W}{P_I}\right)^{-1} + C_3\left(\frac{P_W}{P_I}\right) + C_4 \quad (8)$$

Coefficients C_1 through C_4 were calculated at each Δx step from specified and measured quantities in the square brackets. Quantities specified at all Δx steps are $g = 9.81$ m s^{-2}, $\rho_I = 917$ kg m^{-3}, $\rho_W = 1000$ kg m^{-3}, $n = 3$ (Glen 1955), $m = 2$ (Weertman 1957a), $A = 8$ bar $a^{1/3} = 250$ MPa $s^{1/3}$ for ice at -30°C (Hooke 1998, fig. 11.5), and $B = 0.02$ bar $a^{1/2}$ $m^{-1/2}$ (Wilch & Hughes 2000). The value of B contained in C_4 is not critical because the term containing C_1 is the dominant variable in Eq. 8. Measured quantities at the grounding line and each Δx step are given in Scofield (1988) and Scofield *et al*. (1991). They are $\Delta h/\Delta x$, h_I, w, and u, where $u = u_s$ is assumed and from which $\dot{\varepsilon}_{xx}$, $\dot{\varepsilon}_{yy}$, and $\dot{\varepsilon}_{xy}$ are calculated, and $\dot{\varepsilon}_{xz} = 0$ when $u = u_s$ in Eq 3.

Results

The proper value of τ_S in resisting gravitational flow of Byrd Glacier is unclear. Along the sides of the flowband in Fig. 2, $\tau_S \approx 0$, but along the sides of Byrd Glacier inside the fjord, $\tau_S \approx 250$ k Pa (Whillans *et al*. 1989). Whillans & Van der Veen (1997) maintain that τ_S is the dominant stress for Ice Stream B (now Whillans Ice Stream) in West Antarctica, where $\tau_S \approx 250$ kPa as well. However, they used a force balance that did not include gravitation forcing provided by basal buoyancy and which is linked to P_W/P_I in our

https://doi.org/10.1017/S0954102003001664 Published online by Cambridge University Press

treatment. Zhao (1990) showed that side shear can lead to shear rupture in the lateral shear zones of Byrd Glacier, in which case $\tau_S = 0$ if lateral decoupling is complete.

To check the possibility that τ_S is the major stress resisting gravitational flow of Byrd Glacier, we solved Eqs 2 & 7 for variable flowband width, but retaining only the term that contains τ_S, so that $\Delta h/\Delta x$ depends only on τ_S for known w variations along x. Figure 4 gives the τ_S variations along x using measured variations of $\Delta h/\Delta x$ and w. Flowband width has an effect where the flowband narrows markedly as ice approaches the fjord. However, the major result is the extreme variations of τ_S along x. These variations have no known physical justification in terms of reasons for the radical changes in lateral ice coupling to the fjord walls that would be required. Maxima in τ_S occur at maxima in the surface slope for grounded ice ($x > 0$) and maxima in ice thickness for floating ice ($x < 0$). When terms containing P_W/P_I were included, variations in P_W/P_I fell within the theoretical range $0 < P_W/P_I < 1$ when A = 8 bar $a^{1/3}$. In this case, the term containing τ_S is negligible even if $\tau_S = 250$ kPa is specified.

We calculated the variation of P_W/P_I along x in two ways. In the first calculation, we solved Eq. 7 to match the calculated $\Delta h/\Delta x$ variations along x with the observed variations when each right-hand term was included in sequence to obtain a best-fit variation of P_W/P_I for each step in the sequence using τ_S = 250 kPa at all steps, as determined by Whillans *et al.* (1989). Our goal was to determine the contribution to $\Delta h/\Delta x$ from each term. As seen in Fig. 5, the first and second right-hand terms generally contribute about 70% and 25% respectively, to the observed $\Delta h/\Delta x$ variations, whereas the third and fourth terms that contain τ_S and τ_O respectively, make a combined contribution that is usually about 5%, but can be up to 20%. In the second calculation, we solved Eq. 8 using the observed $\Delta h/\Delta x$ variations to compute $\Delta(P_W/P_I)/\Delta x$ variations directly, and integrated these variations numerically to obtain P_W/P_I variations in the theoretical range $0 < P_W/P_I = 1$, with $P_W/P_I = 1$ at the grounding line as a boundary condition. In Eq. 7, the first right-hand term contains σ_T as the primary component and the contribution of ice-thickness gradient $\Delta h_I/\Delta x$ to $\Delta\sigma_T/\Delta x$ as a secondary component, and the second right-hand term is the contribution of $\Delta(P_W/P_I)^2/\Delta x$ to $\Delta\sigma_T/\Delta x$. Therefore, σ_T is substantially more important than its longitudinal gradient.

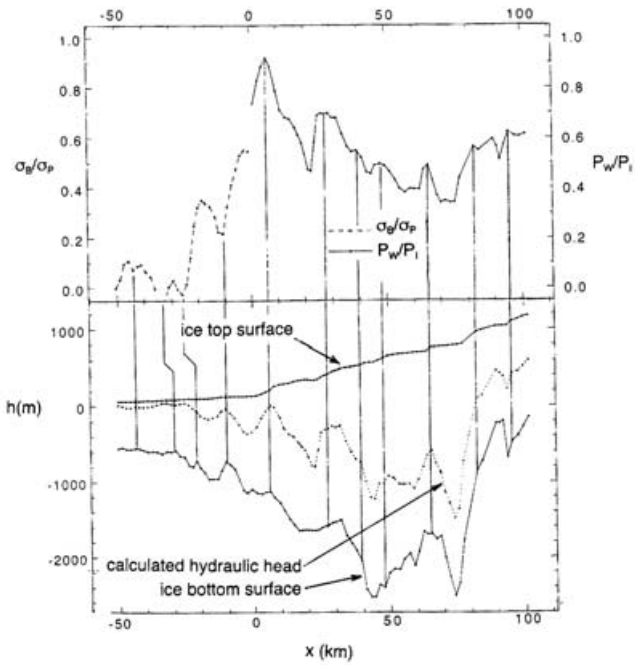

Fig. 6. Variations of ratio σ_B/σ_P of ice-shelf buttressing stress to gravitational pulling stress along the floating length of Byrd Glacier and of ratio P_W/P_I of basal water pressure to ice overburden pressure along the grounded length of Byrd Glacier. Top: Variations of σ_B/σ_P (dashed line) and P_W/P_I (solid line) along the flightline in Fig. 3. Bottom: Surface and bed profiles (solid lines) and calculated hydraulic heads (dashed line) allowed by P_W/P_I along the flightline in Fig. 3.

For the floating part of Byrd Glacier, following Van der Veen (1999, pp. 162–167), x and u_O are positive in Eq. 2. The expression for σ_T derived by Thomas (1973a, 1973b) for ice-shelf buttressing is obtained in Eq. 1 if the following substitution is made to account for the fact that $P_W/P_I = 1$ everywhere but along the fjord sidewalls and at local grounding points, in which cases $P_W/P_I = 0$ (Hughes 1998, p. 56):

$$\frac{P_W}{P_I} = \frac{\rho_W h_W}{\rho_I h_I} = \left(\frac{\sigma_P - \sigma_B}{\sigma_P}\right)^{1/2} \tag{9}$$

where $\sigma_T = \sigma_P$ is the gravitational pulling stress in the x direction for $P_W/P_I = 1$ in Eq. 1:

$$\sigma_P = \frac{\rho_I g h_I}{2 + (\dot{\varepsilon}_{yy}/\dot{\varepsilon}_{xx})}\left(1 - \frac{\rho_I}{\rho_W}\right) \tag{10}$$

For longitudinal flow in the x direction, σ_P is least when $\dot{\varepsilon}_{xx} = \dot{\varepsilon}_{yy}$ for an unconfined ice shelf (Weertman 1957b), and σ_B is the buttressing stress provided by a partly confined ice shelf (Thomas 1973a, 1973b), such as the Ross Ice Shelf which buttresses Byrd Glacier. As a first approximation:

$$\sigma_B = f_G\, \sigma_P \tag{11}$$

where f_G is the fraction of the ice-shelf perimeter that is grounded beyond the grounding line of Byrd Glacier, including local grounding around ice rises and islands. Then $\sigma_B = 0$ for a freely-floating ice shelf ($f_G = 0$) and $\sigma_B = \sigma_P$ for an ice shelf grounded around its entire perimeter ($f_G = 1$), such as ice floating on subglacial Lake Vostok in East Antarctica (Kapista *et al.* 1996). Variations of σ_B on the

https://doi.org/10.1017/S0954102003001664 Published online by Cambridge University Press

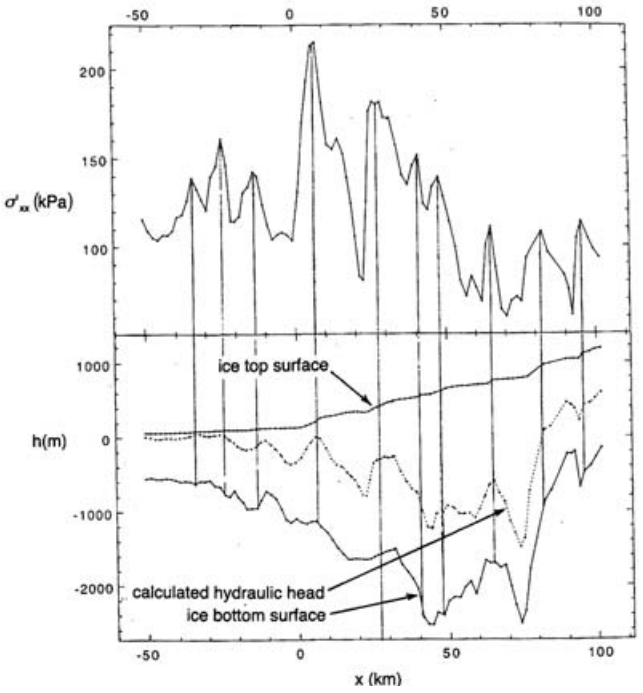

Fig. 7. Variations of longitudinal deviator stress needed to produce observed surface slopes along Byrd Glacier. Top: Variations of longitudinal deviator stress $\sigma'_{xx} = \sigma_T/2$ obtained by applying Eqs 12 & 13 to the P_W/P_I and σ_B/σ_P variations in Fig. 6 along the flightline in Fig. 3. Bottom: Surface and bed profiles (solid lines) along the flightline in Fig. 3, and the elevation of the hydraulic head (dashed line). This elevation is positive above sea level and negative below sea level.

Ross Ice Shelf, which buttresses Byrd Glacier, were determined by Thomas & MacAyeal (1982) and by Jezek (1984). The longitudinal tensile stress obtained by applying Eqs 9 & 10 to Eq. 1 for Byrd Glacier are, for grounded ice:

$$\sigma_T = \frac{\rho_I g h_I}{2 + \left(\dot{\varepsilon}_{yy}/\dot{\varepsilon}_{xx}\right)}\left(1 - \frac{\rho_I}{\rho_W}\right)\left(\frac{P_W}{P_I}\right)^2 = \sigma_P\left(\frac{P_W}{P_I}\right)^2 \qquad (12)$$

and for floating ice:

$$\sigma_T = \frac{\rho_I g h_I}{2 + \left(\dot{\varepsilon}_{yy}/\dot{\varepsilon}_{xx}\right)}\left(1 - \frac{\rho_I}{\rho_W}\right) - \sigma_B = \sigma_P\left(1 - \frac{\sigma_B}{\sigma_P}\right) \qquad (13)$$

Equations 12 & 13 originally derived by Hughes (1992) and Thomas (1973a, 1973b), respectively.

Figure 6 shows variations of P_W/P_I and σ_B/σ_P along x for the respective grounded and floating parts of Byrd Glacier. Taking A = 8 bar $a^{1/3}$ allows $P_W/P_I = 1$ to be approached as a boundary condition at the grounding line where x = 0 and ice velocity attains a maximum of 850 m a^{-1}, before slowing slightly and then increasing again as ice leaves the fjord (Brecher 1982). Over this distance, σ_B/σ_P decreases to nearly zero inside the fjord and remains low beyond the fjord, so the slightly compressive flow can be attributed to ice-shelf buttressing caused by the fjord sidewalls, where $P_W/P_I = 0$. Both P_W/P_I and σ_B/σ_P show irregular variations along x inside the flowband in Fig. 3. Maxima in P_W/P_I occur at inflection points in the surface slope that separate upslope convex surfaces characteristic of sheet flow from downslope concave surfaces characteristic of stream flow. Seven such inflection points combine to give the grounded part of Byrd Glacier the overall concave profile of stream flow. The separation of inflection points ranges from 6 km to 16 km, with an average of 11 km. Minima in σ_B/σ_P are close to minima in ice thickness along the floating part of Byrd Glacier. Four minima are shown. The separation of minima ranges from 8 km to 12 km, with an average of 10 km. Two minima in σ_B/σ_P do not align well with minima in h_I. This may reflect partial grounding of the thicker ice immediately upslope, which tends to align h_I on the lee side of partially grounded ice with a rapid decrease of σ_B/σ_P instead of σ_B/σ_P minima. Alternatively, it may reflect the ad-hoc representation of σ_B implied by Eq. 11. Note that $\sigma_B/\sigma_P \rightarrow 0$ as ice leaves the fjord, indicating that $\sigma_T = \sigma_P$ in Eq. 13 for unconfined shelf flow beyond the fjord. Here lateral fractures through the whole ice thickness largely uncouple Byrd Glacier from the Ross Ice Shelf for some 40 km beyond the fjord entrance, as seen in Fig. 2.

Figure 7 shows the variation of σ'_{xx} along x in Eqs 12 & 13, for which $\sigma_T = 2\sigma'_{xx}$ when $\dot{\varepsilon}_{yy} = 0$ (Hughes 1998, pp. 53–54). In Fig. 7, maxima in σ'_{xx} occur at maxima in P_W/P_I for grounded ice and maxima in ice thickness for floating ice. These maxima are regions where $\dot{\varepsilon}_{xx}$ should be greatest, according to Eq. 4. Therefore, Eq. 13 does not capture the slightly compressive flow for ice floating inside the fjord. This is a region of high basal melting rates that were not included when converting Eq. 2 to Eq. 7, from which our calculation of σ_B/σ_p and therefore our σ'_{xx} values, were obtained. This gives us less confidence in our results for floating ice than for grounded ice. The basal melting rates for floating ice are considerable. Using the velocity and elevation data by Brecher (1982) and calculating ice thickness from ice elevations using the buoyancy requirement for floating ice, the total ice flux for Byrd Glacier in 1979 was 27 km^3 a^{-1} across the grounding line and 15 km^3 a^{-1} across the downstream fjord entrance 50 km beyond the grounding line. The map-plane area over this distance is 1450 km^2, giving a basal melting rate of 8.3 m a^{-1} compared to a measured surface mass balance that is negligible. High basal melting rates, especially non-uniform rates, may account for the variations of floating ice thickness in Fig. 7. The surface expression of ice-thickness minima appears as transverse depressions in Landsat imagery (Lucchitta & Ferguson 1986). Longitudinal compression becomes extension as floating ice leaves the fjord (Brecher 1982, Zhao 1990), beyond which $\sigma_B/\sigma_P \approx 0$ in Fig. 6. We must therefore allow the possibility that floating ice is partly grounded at sites where σ_B/σ_P is

https://doi.org/10.1017/S0954102003001664 Published online by Cambridge University Press

greatest inside the fjord, and this may lead to non-uniform basal melting rates and compressive flow. Our one-dimensional flow model is incapable of capturing this kind of behaviour, except by inference.

Discussion

Our primary conclusion is that Byrd Glacier converts sheet flow in East Antarctica into shelf flow on the Ross Ice Shelf by way of stream flow, in which P_W/P_I increases irregularly along the length of Byrd Glacier from being negligible for sheet flow to unity for shelf flow. This is opposite from the conclusion by Van der Veen (1999, p. 43) that Byrd Glacier is frozen to its bed with zero basal sliding, based on his assessment of the force balance by Whillans *et al*. (1989). In that force balance, the gravitational driving force is linked only to the surface slope and thickness of ice, whereas the gravitational driving force in our force balance is also linked to the thickness of ice that is supported by basal water pressure P_W and to the freeboard height of ice above a longitudinal back-pressure of 1/2 P_W at the grounding line (Hughes 1992, 1998, pp. 51–55). In both force balances, resistance to flow of ice is provided by a basal shear force, a side shear force, and a longitudinal tensile force that are the respective stresses τ_O, τ_S, and σ_T multiplied by the respective basal, side, and transverse areas of Byrd Glacier or of a flowband within Byrd Glacier. Since the basal area is greatest, the side area is much smaller, and the transverse area is smallest of all, roughly in the ratio 125:20:5 for ice grounded between the fjord walls, τ_O will dominate the resistive stresses if the bed is frozen and Byrd Glacier cannot be transitional from sheet flow to shelf flow in the sense of providing progressive ice-bed uncoupling as P_W/P_I increases toward unity. For that to happen, both τ_O and τ_S must be negligible compared to σ_T, which is the dominant stress resisting unconfined shelf flow and, along with τ_O for basal sliding in our treatment, depends on P_W/P_I for grounded ice. However, $\tau_O << \sigma_T$ for values of P_W/P_I that we calculated by matching observed and calculated surface slopes, specifically the wave-like form. In addition, τ_S has little effect in producing this match, regardless of whether we take τ_S = 250 kPa along the fjord walls as obtained by Whillans *et al*. (1989) or, more reasonably, $\tau_S \rightarrow 0$ along the sides of the flowband in Fig. 3. Large variations in τ_S are needed to capture the surface "waves." These variations are without a reasonable physical explanation.

Our results for Byrd Glacier show that longitudinal deviatoric tensile stress σ_T, by incorporating pressure ratio P_W/P_I in the grounded portion and buttressing stress σ_B in the floating portion, plus buttressing by water back-pressure from the ice-shelf calving front to the grounding line, provides the major resistance to gravitational flow for the ice flowband shown in Fig. 3. This is in direct contrast to the conclusion by Whillans *et al*. (1989) that basal shear stress τ_O in grounded ice and side shear stress τ_S in floating ice provide more resistance for the entire width of Byrd Glacier inside the fjord. In addition they, Scofield (1988), and Scofield *et al*. (1991) obtain a high basal shear stress τ_O and a frozen bed at "sticky spots" in the region where Byrd Glacier is grounded, whereas we find that τ_O is small and the bed is largely thawed with a generally high basal water pressure such that $0.3 < P_W/P_I < 1.0$ in incremental area w Δx within which P_W/P_I is a statistical average of $P_W/P_I \rightarrow 1$ in thawed patches dominated by basal melting, $P_W/P_I \rightarrow 0$ in thawed patches dominated by basal freezing, and $P_W/P_I = 0$ in frozen patches. The "sticky spots" are really "slippery spots" where P_W/P_I is high in our analysis. Peaks in P_W/P_I coincide with maxima in the surface slope because these are sites of maximum ice-bed uncoupling, hence sites where the overlying ice is being downdrawn most rapidly. Downdraw due to ice-bed uncoupling also produces maxima in the ice-thickness gradient of ice shelves at their grounding lines, as Van der Veen (1983, 1999, pp. 162–167) shows. These striking differences in τ_O for grounded ice arise from different approaches to the force balance. Whillans *et al*. (1989) allow gravitational forcing linked only to the surface slope, which is the case for sheet flow, whereas we link gravitational forcing to both surface slope for sheet flow (Nye 1953) and to basal buoyancy for shelf flow (Weertman 1957b), because we think that stream flow is transitional from sheet flow to shelf flow (Hughes 1992). Our treatment of shelf flow ignores high basal melting rates and therefore incorporates σ_B in a manner that makes interpreting our results problematic. Maxima in σ'_{xx} are crudely correlated with maxima in h_I for floating ice, which is reasonable, but the h_I maxima exist in a region of mildly compressive flow.

The most puzzling aspect of the irregular behaviour of P_W/P_I is that maxima in P_W/P_I coincide with maxima in ice surface slope that have no clear relationship to the bed slope or to bed topography. Perhaps the maxima in surface slope are not "anchored" to bed topography, but are migrating either upslope or downslope over time. The rather uniform spacing of these maxima implies that any such migration is all one way, not both ways. Upslope migration implies inland migration of basal water, hence of ice-bed uncoupling, to produce an inwardly migrating "wave train" of maxima in the surface slope. This may be the "surge" mechanism proposed by Hughes (1975) for West Antarctic ice streams, analysed by Robin & Weertman (1973), modelled by Campbell & Rasmussen (1970), and observed by Bindschadler (1997) on West Antarctic ice streams, especially Whillans Ice Stream. In that case, there would be one "surge" for each maximum in the surface slope of Byrd Glacier. In Fig. 6, the hydraulic head is calculated from $h_W = (\rho_I/\rho_W)(P_W/P_I)\, h_I$, using Eq. 9. Unlike peaks in P_W/P_I, peaks in h_W are associated with peaks in basal topography, which suggests that basal meltwater is produced at these sites by fast-moving ice that causes high rates of pressure melting at the bed. In this case, pressure melting due to fast ice flow at bedrock peaks exceeds pressure melting due to

https://doi.org/10.1017/S0954102003001664 Published online by Cambridge University Press

the greater thickness of slower ice in bedrock valleys, and the surface "wave train" is anchored to these bedrock highs as a series of "standing waves." However, basal melt water should flow down the hydraulic gradient in Fig. 6, which may allow both upslope and downslope migration of the maxima in surface slope as "travelling waves" until these maxima conform more to the maxima in the hydraulic head (Paterson 1994, pp. 110–114). In fact, h_W tends to be rather constant along the grounded length of Byrd Glacier, compared to the variation of P_W/P_I, indicating that this pattern of basal water flow exists. This flow tends to increase h_W where the surface slope is high and decrease h_W where the surface slope is low, as Paterson (1994, pp. 110–114) requires.

Upslope migration of basal water would thin the ice and make the grounding-line retreat, whereas downslope migration would thicken the ice and make the grounding line advance. If P_W/P_I is not a source of gravitational forcing in Byrd Glacier, LeMeur & Hindmarsh (2001) and Hindmarsh & LeMeur (2001) show that the relationship between ice-thickness changes and grounding-line migration is not self-evident. Eric Rignot (personal communication 2002) reports an ice flux of 23.5 $km^3\ a^{-1}$ across the grounding line in 1997, compared to a mass-balance ice flux of about 44 $km^3\ a^{-1}$, which should cause Byrd Glacier to thicken and the grounding line to advance, according to Thomas (1977). However, Rignot & Jacobs (2002) calculate a basal melting rate of 15 ± 4 m a^{-1} near the grounding line, which should cause it to retreat. They also locate the 1997 grounding line some 20 km further inland from where Hughes & Fastook (1981) located it in 1979.

It seems possible that Byrd Glacier may be undergoing rapid changes. Modelling these changes will require accurate bed topography in the map plane, a new map of the ice surface to detect migrations of the grounding line and of maxima in the surface slope, and a three-dimensional model of ice dynamics that includes subglacial hydrology and P_W/P_I as a major variable linked to changes in hydrology over time. Our conclusions depend on basal buoyancy being responsible for gravitational forcing, in addition to surface slope, for stream flow. There is no general consensus that this is the case. We hope our study will stimulate further research. In particular, drilling a series of boreholes upslope from the grounding line of an ice stream would be required to see if P_W/P_I varies upslope in a way that is compatible with gravitational forcing that includes basal buoyancy. The drilling program for Siple Coast ice streams in West Antarctica did not include this crucial experiment. Drilling these holes upslope for Byrd Glacier would confront heavy crevassing and ice over 3 km thick in places.

Finally, an explanation of P_W variations in the ratio P_W/P_I is necessary to avoid the false conclusion that basal water pressure is typically less than the ice overburden pressure beneath Byrd Glacier, and the bed is always thawed. In fact, $P_W = \rho_W\, g\, h_W$, so P_W is a measure of how much basal water is available to rise to height h_W in a hypothetical borehole to the bed. If the bed is frozen, $h_W = P_W/P_I = 0$. If little water is present on a thawed bed, h_W will be small and $P_W/P_I \rightarrow 0$. If much basal water is present, h_W will be close to the height needed to float the ice overburden and $P_W/P_I \rightarrow 1$. Therefore, the correct way to understand P_W/P_I variations in Fig. 6 is to see the bed as a mosaic of frozen and thawed patches, with poor hydraulic conductivity from thawed patches having much water to thawed patches having little water. Then the P_W/P_I variations in Fig. 6 are a statistical distribution of sites in incremental area w Δx of the bed where the bed is frozen ($P_W/P_I = 0$), thawed with little water ($P_W/P_I \rightarrow 0$), and thawed with much water ($P_W/P_I \rightarrow 1$). The average of these individual P_W/P_I values is the P_W/P_I value that appears in Fig. 6 for area w Δx at distance x upslope from the grounding line. Similarly the variations of hydraulic head $h_W = (\rho_I/\rho_W)\ (P_W/P_I)\ h_I$ in Figs 6 & 7 represent the tortuous flow of basal water from more wet to less wet thawed patches, while avoiding frozen patches. Our results then support the conclusion by Scofield (1988), Scofield *et al*. (1991), and Whillans *et al*. (1989) that some parts of the bed under Byrd Glacier are frozen and other parts are thawed, and illuminate the nature of subglacial hydrology for this type of bed. In thawed parts of the bed, we conclude that basal water flows from sites of basal melting (high P_W/P_I) to sites of basal freezing (low P_W/P_I).

Acknowledgements

This work was conducted under NSF grant OPP-9900477. We thank Dr Richard Hindmarsh and an unnamed referee for their constructive comments.

References

Bindschadler, R. 1997. Actively surging West Antarctic ice streams and their response characteristics. *Annals of Glaciology,* **24**, 409–414.

Brecher, H.H. 1982. Photographic determination of surface velocities and elevations on Byrd Glacier. *Antarctic Journal of the United States,* **17**(5), 79–81.

Campbell, W.J. & Rasmussen, L.A. 1970. A heuristic numerical model for three-dimensional time-dependent glacier flow. *International Association of Hydrologic Sciences Publication,* **86**, 177–190.

Glen, J.W. 1955. The creep of polycrystalline ice. *Proceedings of the Royal Society of London*, **A228**, 519–538.

Hindmarsh, R.C.A. & Lemeur, E. 2001. Dynamics processes involved in the retreat of marine ice sheets. *Journal of Glaciology,* **47**, 271–282.

Hooke, R.L. 1998. *Principles of glacier mechanics*. Upper Saddle River, NJ: Prentice-Hall, 248 pp.

Hughes, T. 1975. The West Antarctic Ice Sheet: instability, disintegration, and initiation of ice ages. *Reviews of Geophysics and Space Physics,* **13**, 502–526.

Hughes, T. 1979. Byrd Glacier. *Antarctic Journal of the United States,* **14**(5), 88–91.

Hughes, T. 1992. On the pulling power of ice streams. *Journal of Glaciology,* **38**, 125–151.

Hughes, T. 1998. *Ice sheets*. New York: Oxford University Press, 343 pp.

Hughes, T.J. & Fastook, J.L. 1981. Byrd Glacier: 1978–1979 field results. *Antarctic Journal of the United States,* **16**(5), 86–89.

https://doi.org/10.1017/S0954102003001664 Published online by Cambridge University Press

JEZEK, K.C. 1984. A modified theory of bottom crevasses used as a means for measuring the buttressing effect of ice shelves on inland ice sheets. *Journal of Geophysical Research,* **89**(B3), 1925–1931.

JEZEK, K.C., *ed*. 1998. *Early results from the first RADARSAT-1 Antarctic Mapping Mission*. Byrd Polar Research Center Technical Report 98-02, Byrd Polar Research Center, The Ohio State University, 22 pp.

KAPITSA, A.P., RIDLEY, J.K., ROBIN, G. DE Q., SIEGERT, M.J. & ZOTIKOV, I.A. 1996. A large deep fresh-water lake beneath the ice of central East Antarctica. *Nature,* **381**, 684–686.

LEMEUR, E. & HINDMARSH, R.C.A. 2001. Coupled marine-ice-sheet/Earth dynamics using a dynamically consistent ice-sheet model and a self-gravitation viscous Earth model. *Journal of Glaciology,* **47**, 258–270.

LUCCHITTA, B.K. & FERGUSON, H.M. 1986. Antarctica: measuring glacier velocity flow from satellite images. *Science,* **234**, 1105–1108.

NYE, J.F. 1953. The flow law of ice from measurements in glacier tunnels, laboratory experiments and the Jungfraufirn borehole experiment. *Proceedings of the Royal Society of London*, **A219**, 477–489.

PATERSON, W.S.B. 1994. *The physics of glaciers*. Oxford: Pergamon Publishing. 480 pp.

RIGNOT, E. & JACOBS, S. 2002. Rapid bottom melting widespread near Antarctic Ice Sheet grounding lines. *Science*, **296**, 2020–2023.

ROBIN, G. DE Q. & WEERTMAN, J. 1973. Cyclic surging of glaciers. *Journal of Glaciology,* **12**, 3–18.

SCOFIELD, J.P. 1988. *Flow characteristics of an outlet glacier: Byrd Glacier*, *Antarctica*. MSc thesis, University of Maine, 146 pp. [Unpublished]

SCOFIELD, J.P., FASTOOK, J.L. & HUGHES, T. 1991. Evidence for a frozen bed, Byrd Glacier, Antarctica. *Journal of Geophysical Research,* **96**(B7), 11 649–11 655.

THOMAS, R.H. 1973a. The creep of ice shelves: theory. *Journal of Glaciology,* **12**, 45–53.

THOMAS, R.H. 1973b. The creep of ice shelves: interpretation of observed behaviour. *Journal of Glaciology,* **12**, 55–70.

THOMAS, R.H. 1977. Calving bay dynamics and ice sheet retreat up the St Lawrence valley system. *Géographie Physique et Quaternaire,* **31**, 347–356.

THOMAS, R.H. & MACAYEAL, D.R. 1982. Derived characteristics of the Ross Ice Shelf. *Journal of Glaciology,* **28**, 397–412.

VAN DER VEEN, C.J. 1983. *A note on the equilibrium profile of a free floating ice shelf*. Rijksuniversiteit-Utrecht, The Netherlands: Institut voor Meteorologie en Oceanografie, 83–15, 15 pp.

VAN DER VEEN, C.J. 1999. *Fundamentals of glacier dynamics*. Rotterdam: Balkema, 462 pp.

WEERTMAN, J. 1957a. On the sliding of glaciers. *Journal of Glaciology,* **3**, 33–38.

WEERTMAN, J. 1957b. Deformation of floating ice shelves. *Journal of Glaciology,* **3**, 38–42.

WHILLANS, I.M., CHEN, Y.H., VAN DER VEEN, C.J. & HUGHES, T. 1989. Force Budget III: Application to three-dimensional flow of Byrd Glacier, Antarctica. *Journal of Glaciology,* **35**, 68–80.

WHILLANS, I.M. & VAN DER VEEN, C.J. 1997. The role of lateral drag in the dynamics of Ice Stream B, Antarctica. *Journal of Glaciology,* **43**, 231–237.

WILCH, E. & HUGHES, T. 2000. Mapping basal thermal zones beneath the Antarctic ice sheet. *Journal of Glaciology,* **46**, 297–310.

ZHAO, Z. 1990. *Measurement, analysis, and modelling of deformation of the shelf-flow, Byrd Glacier*. PhD thesis, University of Maine, 108 pp. [Unpublished]

https://doi.org/10.1017/S0954102003001664 Published online by Cambridge University Press